

# Equivalent Magnetization Current Method Applied to the Design of Gradient Coils for Magnetic Resonance Imaging

Hector Sanchez Lopez, Feng Liu, Michael Poole, and Stuart Crozier

School of Information Technology and Electrical Engineering, University of Queensland, QLD, Australia

A new method is described for the design of gradient coils for magnetic resonance imaging systems. The method is based on the known equivalence between a magnetized volume surrounded by a conducting surface and its equivalent representation by a surface current density. The curl of a vertical magnetization vector of a magnetized thin volume is equivalent to a surface current density whose stream line defines a coil current pattern. This concept is applied to the design of gradient coils of arbitrary shape. The thin magnetized volume is discretized in small triangular elements. By calculating the contribution of each magnetized block at target points a field source matrix is obtained. The equivalent magnetization current concept is applied to obtain the equivalent coil impedance, force and torques. A quadratic programming optimization algorithm is used to obtain the stream-magnetization-thickness function value at each node such that coils of optimal performance are obtained. This method can be used for gradient coils wound on arbitrary surface shapes and can be applied to hybrid current/iron solutions. A variety of examples are shown to demonstrate the versatility of the method. A novel partially shielded 3-D biplanar gradient coil for open MRI magnets is presented.

**Index Terms**—Biplanar gradient coil design, magnetic resonance imaging (MRI), three-dimensional gradient coil structure.

## I. INTRODUCTION

THE characteristics of gradient coils are critical for modern magnetic resonance imaging (MRI) applications. Many methods based on different optimization techniques and modeling approaches [1]–[12] have been presented with the purpose of finding current patterns able to generate a highly efficient gradients ( $\eta$ , gradient per unit current measured in T/m/A) with low stored magnetic energy (low inductance  $L$ ,  $\mu\text{H}$ ) and linear axial magnetic field intensity along each Cartesian dimension within the imaging region, also known as the diameter spherical volume (DSV).

Fast imaging experiments, such as echo-planar imaging (EPI) [13], together with patient comfort levels and reduced MRI system length are some examples of requirements that provide additional challenges to gradient coil design. More open access to the imaging volume reduces claustrophobia in patients and also enables better interaction between the medical attendant and the patient. It would be desirable to design coils with as large a radius as possible to enable better access to the DSV. Coil performance however, often measured as the ratio  $\eta^2/L$  [3], decreases dramatically when the coil radius is increased. For constant efficiency and winding configuration the inductance depends on the fifth power of the radius. However, the magnetic field strength falls rapidly with distance from a current element; hence gradient coils must be as close as possible to the region of interest. Unfortunately, magnetic field sources must be placed at a distance from the DSV to fulfill the linearity condition of the magnetic field in the DSV. Hence, an optimal compromise must be reached among all of these competing factors.

Small radii head-gradient coils perform better than whole body coils when a small sample, such as a human head, is to

be imaged [14]–[20]. Dedicated head gradient coils can reduce peripheral nerve stimulation (PNS) in the rest of the body as well as the inductive interaction between the coil and the surrounding metallic structure; lower net Lorentz forces are produced and hence lower acoustic noise may be generated. When a coil with a small length-to-diameter ratio is required, large concentrations of wires usually appear at the ends of the coil increasing the cooling and construction problems.

If the solutions produced by conventional methods are grouped by geometry (e.g., cylindrical) and gradient coil type (e.g., transverse), the current topology pattern is found to be similar in almost all the cases. The resulting solutions show a current pattern where the main current and the returning current arcs are often placed on the same surface. As a consequence, when the coil dimensions are reduced, the main and return arcs are located close to the DSV. The mathematics of conventional methods developed for specific geometries (e.g. hyperbolic, spherical, cylindrical or planar) require surfaces that exhibit a high degree of symmetry, which constrains the ability to explore novel gradient coil geometries. The demand of new trends in MRI system design necessitates the need to explore new and creative geometries and hence to obtain novel gradient coil designs. A recently presented approach assumed coaxial surfaces were conjoined by a conical surface [11]. Current was allowed to flow from the primary surface to the shielding surface, along straight lines on a connecting conical surface. The merit of this method is in the possibility of producing ultra-short cylindrical shielded gradient coils by utilizing some of the return path wires for active magnetic shielding purposes.

Coil design methods developed in discrete real space [21], [22] offer some advantages with respect to those approaches developed for a particular geometry. These methods rely on deformable parametric curves that represent the coil pattern and can be applied to arbitrary geometries. For each problem, however a new and appropriate parametric curve has to be found.

In order to overcome this limitation some methods, independent of the shape of the current-carrying surface, have been presented. Pissanetzky introduced a coil design method in which an arbitrary surface is discretized into small mesh patches and for

Manuscript received June 23, 2008; revised November 05, 2008. Current version published February 11, 2009. Corresponding author: H. Sanchez Lopez (e-mail: hsanchez@itee.uq.edu.au).

Color versions of one or more of the figures in this paper are available online at <http://ieeexplore.ieee.org>.

Digital Object Identifier 10.1109/TMAG.2008.2010053

each of these elements, a current flow formulation, known as the stream function, is defined [23]. In 2003, Peeren [24] presented a detailed mathematical treatment of the method presented by Pissanetzky and extended it to general electromagnetic problems. Lemdiasov and Ludwig presented the Pissanetzky basis function through a compact mathematical expression [25]. More recently, it was demonstrated that by combining the Pissanetzky method with mesh generator software, new geometries and solutions can be explored [26].

In this paper, we present a new gradient coil design method that is independent of the shape of the current-carrying surface. The surface does not need to be simple, nor connected because the method is based on the equivalence between a magnetized volume and a surface current density. A three-dimensional thin volume is discretized in small patches in which magnetization is directed parallel to the direction of the normal to the surface. Formulating the magnetization distribution in this way is equivalent to the stream function of the current density that defines the coil current pattern. By applying the Equivalent Magnetization Current (EMC) (fictitious “magnetization” currents) method the equivalent magnetic energy, delivered power, force and torque can be obtained. We demonstrate the success of this approach through worked examples, where the similarities and differences with respect to Pissanetzky’s method are discussed. The new methodology is simple to implement and opens the possibility of exploring new structures and hence produces novel gradient coil solutions.

## II. MATERIALS AND METHODS

In this section the well-known stream function [12], [27] and EMC concepts [28] are presented and applied to the design of gradient coils of arbitrary shapes. The stream-magnetization-thickness function will then be described followed by the EMC implementation for gradient coil design.

### A. Stream Function

From steady state and linear matter, a necessary condition for the current density is deduced

$$\nabla \cdot \mathbf{J} = 0. \quad (1)$$

This means that  $\mathbf{J}(\mathbf{r}')$  can represent the flow of incompressible matter in the source domain  $\Omega$ . Incompressibility means that the movement of matter is restricted to a conservation law that states that no matter is generated or lost in any point at any time. For this reason, the vector field  $\mathbf{J}(\mathbf{r}')$  is also called source-free and can be written as the curl of the current vector potential  $\mathbf{T}(\mathbf{r}')$

$$\mathbf{J}(\mathbf{r}') = \nabla \times \mathbf{T}(\mathbf{r}'). \quad (2)$$

The current vector potential  $\mathbf{T}$  has been extensively used on the simulation of eddy current problems [27]. Details of the properties of the  $\mathbf{T}$ -normal component have been presented in [12] for shim and gradient coil designs.

Assuming the current density flows in a surface  $\mathbf{J} : \Omega \rightarrow \mathfrak{R}^2$ , its vector potential,  $\mathbf{T}$ , has only one component directed

outward, normal to the surface of the domain  $\Omega$ . Then (2) can be expressed as [12]

$$\mathbf{J}_S(\mathbf{r}') = \nabla \times \psi \cdot \hat{\mathbf{n}} \quad (3)$$

where  $\hat{\mathbf{n}}$  is the unit outward pointing normal vector. The surface vector function defined in (3) represents the velocity of incompressible matter. The potential function  $\psi$  is known as the stream function and it is defined in a continuous orientable domain with piecewise differentiable boundary. From (3) it is deduced that a spatial change in the value of  $\psi$  corresponds to an equivalent change in the value of the current density. Contour plots of the function  $\psi$  in the source domain  $\Omega$  represent the locations of the discrete wires carrying equal currents [12].

### B. EMC Method

The magnetic vector potential,  $\mathbf{A}$ , due to a magnetic dipole moment  $d\mathbf{m} = \mathbf{M}dV'$  will produce a vector magnetic potential [28, p. 186]

$$\mathbf{A}(\mathbf{r}) = \frac{\mu_0}{4\pi} \frac{\mathbf{m} \times \mathbf{r}}{|\mathbf{r}|^3} \quad (4)$$

where  $\mu_0 = 4\pi \cdot 10^{-7}$  (H/m) is the permeability of free space and  $\mathbf{r}$  is the distance between the source point and a field point. Although the magnetization  $\mathbf{M}$  is treated as any other field quantity it should be visualized as an average value taken over many molecules; this has the effect of giving the magnetic dipoles a net alignment from their otherwise random orientation. After applying some identities the magnetic vector potential caused by a discontinuous distribution of magnetic dipoles (i.e., a hard ferromagnet) is written as [28]

$$\mathbf{A}(\mathbf{r}) = \frac{\mu_0}{4\pi} \int_{V'} \frac{1}{R} \nabla' \times \mathbf{M}(\mathbf{r}') dV' + \frac{\mu_0}{4\pi} \int_S \frac{\mathbf{M}(\mathbf{r}') \times \hat{\mathbf{n}}}{R} dS \quad (5)$$

where  $R$  is the distance between the source point and a field point. Comparing (5) with the expression of the vector potential, generated by the ordinary current density, it is deduced that  $\nabla' \times \mathbf{M}(\mathbf{r}')$  [28, Eq. 5.79] has the effect of an equivalent volume current density (effective current density), while  $\mathbf{M}(\mathbf{r}') \times \hat{\mathbf{n}}$  has the effect of an equivalent surface current density [28, p. 192].

Let us consider an arbitrary magnetized volume shape bounded by the surface  $S$ . We consider that  $S$  is a connected, piecewise smooth, orientable with a piecewise differentiable boundary.  $S \in \mathfrak{R}^3$ , therefore a normal  $\hat{\mathbf{n}}(\mathbf{r}')$  exists which is piecewise continuously differentiable on  $S$ . We assume an isotropic, rigid, non-hysteresis magnetized volume with magnetization  $\mathbf{M}(\mathbf{r}')$  parallel to the normal vector  $\hat{\mathbf{n}}$ ; hence,  $\mathbf{M}(\mathbf{r}') \times \mathbf{n}(\mathbf{r}') = 0$  in every point  $\mathbf{r}'$ , where  $\hat{\mathbf{n}}(\mathbf{r}')$  is continuously differentiable. Therefore only an equivalent volumetric current density can be used as an equivalent representation of the vertical magnetization  $\mathbf{M}(\mathbf{r}')$ . If we assume that the equivalent magnetization current flows in a thin volume of thickness  $h$  then  $\nabla' \times \mathbf{M}(\mathbf{r}')$  is transformed in an equivalent

current surface  $\mathbf{J}_{\text{Seq}}$  density, and the vector potential (5) can be written as

$$\mathbf{A}(\mathbf{r}) = \frac{\mu_0}{4\pi} \int_S \frac{1}{R} \mathbf{J}_s(\mathbf{r}') dS, \quad \mathbf{r}' \in S \quad (6)$$

where

$$\mathbf{J}_{\text{Seq}}(\mathbf{r}') \approx \nabla' \times \mathbf{M}(\mathbf{r}')h. \quad (7)$$

The subscript eq means equivalent current density. The aforementioned approach is valid if the volume is thick enough to produce a magnetization pointing outward from the surrounding surface and the magnitude and direction of the  $\mathbf{M}$  vector is constant through the thin volume.

Comparing (7) and (3) and from the demonstrated equivalency between magnetized thin volume and a current density that flows over the surface  $S$ , we can write

$$\mathbf{J}_s(\mathbf{r}') \approx \nabla' \times \mathbf{M}(\mathbf{r}')h = \nabla \times \psi(\mathbf{r}') \cdot \hat{\mathbf{n}}(\mathbf{r}') \quad (8)$$

and hence the magnetization-thickness-stream function is written as

$$\mathbf{M}(\mathbf{r}')h \approx \psi(\mathbf{r}') \cdot \hat{\mathbf{n}}(\mathbf{r}'). \quad (9)$$

Equation (8) shows that the curl of a vertical magnetized thin volume is equivalent to a surface current density whose stream line defines the coil current pattern. We apply this concept to the design of gradient coils for MRI.

### C. EMC Method Applied to the Design of Gradient Coils for MRI

The arbitrary geometry of a thin volume is discretized in  $NE$  triangular elements of thickness  $h$  by  $N$  nodes. We assume that only the triangular elements associated to the current node  $n$  induces a magnetization  $\mathbf{M}$ . In the remaining elements the magnetization is zero. It signifies that the basic “building block” is formed for those elements associated with the calculated current node  $n$ . See Fig. 1.

In order to fulfill the continuity (1) it is required that the stream-magnetization-thickness function be set exactly to a constant value on each boundary. Such conditions guarantee that no current will be generated or created at the boundary. This is an essential condition to assure a closed current pattern contour.

We point out that although the magnetization-thickness function ( $\mathbf{M}h$ ) has a constant value in the triangle  $i$ , it may have a different value in the next triangle ( $i+1$ ) associated to the node  $n$ . This spatial change in the “basic block” domain produces an approximated current density whose stream line defines the current pattern. See (8).

### D. Magnetic Field Calculation

Applying the curl operator,  $\nabla \times$ , to (4) we obtain the expression for the magnetic induction field,  $\mathbf{B}$ , produced at a point  $\mathbf{r}$  by a magnetized volume

$$\mathbf{B} = -\frac{\mu_0}{4\pi} \nabla_{\mathbf{r}} \int_{S'} h \mathbf{M} \cdot \nabla_{\mathbf{r}'} \left( \frac{1}{R} \right) dS'. \quad (10)$$

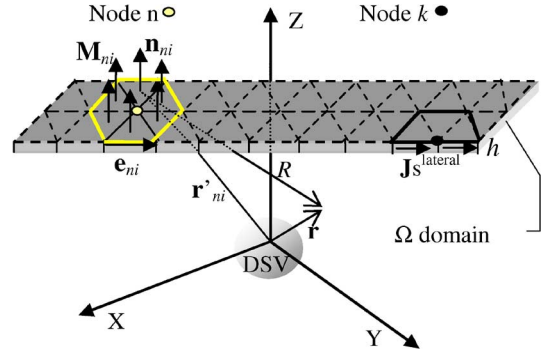


Fig. 1. Coordinates system used in this work. The source vector  $\mathbf{r}'_{ni}$  point at the magnetized element  $i$  associated with the current node  $n$ . In light color (yellow) has been highlighted the  $n$ th “building block” formed for  $O$  triangles;  $i = 1 \dots O$ . A constant value is assigned to all edge nodes  $k$ . The vector  $\mathbf{n}_{ni}$  is the normal of the triangle  $i$  associated with the current node  $n$ .

The magnetic field contribution of all magnetized elements can be calculated assuming the stream function as a sum of the independent amplitudes,  $s_n$ , at each node  $n$

$$\psi(\mathbf{r}') = \sum_{n=1}^N s_n \hat{\psi}_n(\mathbf{r}'), \quad \mathbf{r}' \in S \quad (11)$$

where the function  $\hat{\psi}_n(\mathbf{r}')$  is set to one if the triangle is associated with the current node  $n$ , otherwise it is set to zero. Substituting the magnetization-thickness function, ( $\mathbf{M}(\mathbf{r}')h$ ), for the expression,  $\psi(\mathbf{r}') \cdot \hat{\mathbf{n}}(\mathbf{r}')$ , in (10), we can write

$$\mathbf{B} = -\frac{\mu_0}{4\pi} \sum_{n=1}^N s_n \sum_{i=1}^O \nabla_{\mathbf{r}} \int_A \hat{\psi}_n(\mathbf{r}') \hat{\mathbf{n}}_{ni}(\mathbf{r}') \nabla_{\mathbf{r}'} \left( \frac{1}{R} \right) dA \quad (12)$$

where  $dA$  is the element area of the triangle  $i$ th associated with the node  $n$ .  $s_n$  is the unknown value of the stream function value at the node  $n$ .  $O$  is the number of polygonal elements associated with the current node  $n$ .

In MRI experiments we are usually interested only in the axial component of the magnetic field; from (12) we can express this as

$$B_z(x, y, z) = \sum_{n=1}^N s_n c_n \quad (13)$$

where

$$c_n = -\frac{\mu_0}{12\pi} \sum_{i=1}^O \int_A \left[ \frac{-3(z-z')(x-x')n_{x,ni} - 3(z-z')(y-y')n_{y,ni}}{R_{ni}^5} + \dots \frac{((x-x')^2 + (y-y')^2 - 2(z-z')^2) n_{z,ni}}{R_{ni}^5} \right] dA$$

and  $R_{ni}$  is the distance from the target point  $(x, y, z)$  to the source point  $(x', y', z')$  located in the triangle  $i$  associated with node  $n$ .

### E. Equivalent Magnetic Energy, Power Delivered, Force and Torque Calculation

We have assumed the magnetization-thickness function has a constant value in the triangle  $i$ , hence the magnetization effect can be replaced by an equivalent magnetization surface current density  $\mathbf{J}_S^{\text{lateral}}$  (fictitious “magnetization” current) that flows in the lateral face (at the edge) of the triangle. This vector is defined as

$$\mathbf{J}_S^{\text{lateral}} = \sum_{n=1}^N s_n \sum_{i=1}^O \frac{\mathbf{e}_{ni}}{A_{ni}^{\text{lateral}}} \quad (14)$$

where  $A_{ni}^{\text{lateral}}$  is the lateral area of the element  $i$  associated with the node  $n$ , and  $\mathbf{e}_{ni}$  is the vector of the edge opposite to the node  $n$ . See Fig. 1. The current density  $\mathbf{J}_S^{\text{lateral}}$  flows in the lateral face of the “building block” corresponding to the node  $n$ .

The equivalent stored magnetic energy can be expressed as [28]

$$\begin{aligned} W_{eq} &= \frac{\mu_0}{8\pi} \int_A \int_{A'} \frac{\mathbf{J}_S^{\text{lateral}}(\mathbf{r}) \cdot \mathbf{J}_S^{\text{lateral}}(\mathbf{r}')}{R} dAdA' \\ &\approx \frac{\mu_0}{8\pi} \sum_{n=1}^N \sum_{m=1}^N s_n s_m L_{mn} \end{aligned} \quad (15)$$

where

$$L_{mn} = \sum_{i=1}^O \sum_{j=1}^{O'} \int_A \int_{A'} \frac{\mathbf{e}_{ni} \cdot \mathbf{e}_{mj}}{A_{ni}^{\text{lateral}} \cdot A_{mj}^{\text{lateral}} R_{ni,mj}} dAdA'$$

and  $O$  and  $O'$  are the number of triangles associated with the “building block” of nodes  $n$  and  $m$ , respectively. The equivalent energy expression contains the self and mutual interaction between “building blocks.” Because we have assumed the thickness as a small quantity the surface integral contained in the squared matrix  $L_{mn}$  can be transformed in a line integral over the closed contour defined by the “building block”. In this way the computational burden is reduced.

The equivalent resistance can be expressed in terms of the equivalent surface current density  $\mathbf{J}_S^{\text{lateral}}$  [28]

$$\begin{aligned} R &= \rho_s \int_A \mathbf{J}_S^{\text{lateral}}(\mathbf{r}) \cdot \mathbf{J}_S^{\text{lateral}}(\mathbf{r}') dA \\ &\approx \rho_s \sum_{n=1}^N \sum_{m=1}^N s_n s_m R_{mn} \end{aligned} \quad (16)$$

where

$$R_{mn} = \sum_{i=1}^O \sum_{j=1}^{O'} \int_A \frac{\mathbf{e}_{ni}}{A_{ni}^{\text{lateral}}} \cdot \frac{\mathbf{e}_{mj}}{A_{mj}^{\text{lateral}}} dA$$

and  $\rho_s$  is the surface resistance given in ohm units. As well as (15), the expression (16) contains the self and the mutual resistance between “building blocks”. The value of  $R_{mn}$  is different

from zero if the “building block”  $m$  and  $n$  have common triangles.

The equivalent Lorentz force and the torque acting over the current density  $\mathbf{J}_S^{\text{lateral}}$  in an external magnetic field  $\mathbf{B}_0$  are given by

$$\mathbf{F} = \int_A \mathbf{J}_S^{\text{lateral}}(\mathbf{r}') \times \mathbf{B}_0(\mathbf{r}') dA \quad (17)$$

$$\mathbf{T} = \mathbf{r} \times \mathbf{F}. \quad (18)$$

The equivalent force and torque are linear magnitudes respect at the stream function amplitude  $s_n$ .

As mentioned above, it is desirable that the gradient coil produces a low amount of stored magnetic energy as well as a highly linear magnetic field in the DSV. Hence, the optimization problem can be stated as

$$\begin{aligned} &\min \sum_{n=1}^N \sum_{m=1}^N s_n s_m L_{mn} \\ &\text{subject to} \\ &\sum_{n=1}^N s_n \frac{\partial c_{n,p}}{\partial \mathbf{r}} \leq G_0(1 + \varepsilon) \quad p = 1, \dots, P \\ &-\sum_{n=1}^N s_n \frac{\partial c_{n,p}}{\partial \mathbf{r}} \leq -G_0(1 - \varepsilon) \\ &\sum_{n=1}^N s_n c_{n,p} \leq B_z^{\text{Shield}} \quad p = P + 1, \dots, P + K \\ &-\sum_{n=1}^N s_n c_{n,p} \leq B_z^{\text{Shield}} \quad p = P + 1, \dots, P + K \end{aligned} \quad (19)$$

where  $G_0$  (T/m) is the target gradient field strength specified at  $P$  target points on the surface of the DSV,  $B_z^{\text{Shield}}$  is the maximum desired field value specified on  $K$  points on the target surface. The quantity  $\partial c_{n,p}/\partial \mathbf{r}$  represents the gradient of the magnetic field with respect to position and contains the contribution of each node  $n$  at each target point  $p$ . If a transverse gradient coil is designed then  $\partial c_{n,p}/\partial x$  has to be evaluated. The parameter  $\varepsilon$  allows control over the desired target gradient uniformity and, at the same time, relaxes the boundary conditions in the DSV. Torque and force may be included in (19) which will result in a balanced gradient coil. Alternatively, the square matrix defined in (16) may replace the equivalent stored magnetic energy as an objective function in (19). It is well-known that stored energy minimization techniques result in more oscillatory current density patterns than power dissipation minimization techniques [3] (for equivalent magnetic field inhomogeneity) which increases construction and cooling problems. This is caused by the difference in spatial weighting of the two methods; the power dissipation is weighted by one for nodes that share elements and by zero for all other node pairs, whereas the stored energy between two nodes contains an inverse relationship with respect to the nodal separation. The interaction between two “building blocks” is effective even for far “building block” neighbors. The mutual interaction implicit in the resistance matrix is smaller

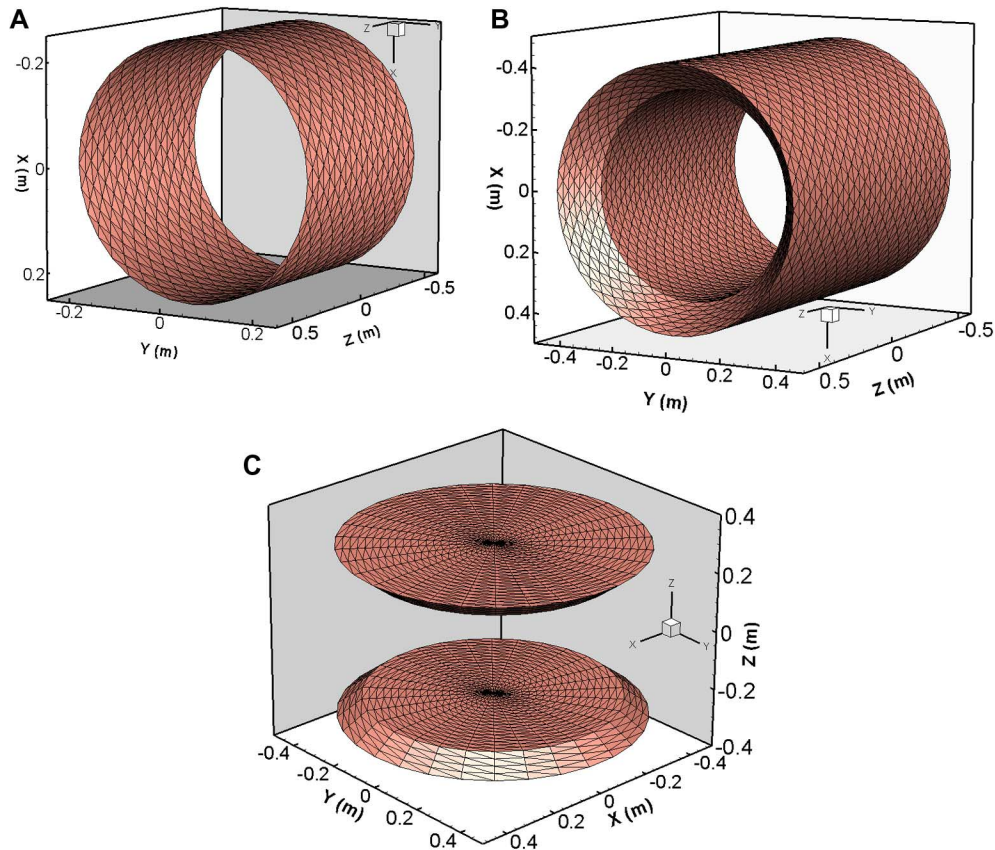


Fig. 2. Geometries and triangular meshes generated using GMSH [32]. The cylinder used for the asymmetric gradient coil (a), an ultra-short shielded gradient coil (b), and the biplanar gradient coil (c).

than the aforementioned coupling. The resistance matrix contains the self interaction and the coupling between consecutive nodes or “building blocks” that shares triangles; hence smoother coil patterns are generated. The topology of the matrix  $L_{mn}$  and  $R_{mn}$  depends on the geometry and both determine the gradient coil current pattern distribution when  $L_{mn}$  or  $R_{mn}$  are used as objective function. The energy and the resistance matrix of coils wound over cylindrical surfaces (not cutout for shoulder [29]) have the same characteristic in regards to the matrix topology; larger or smaller size cylindrical supports only change the amplitude (coupling strength) of the characteristic oscillating modes of the  $L_{mn}$  or  $R_{mn}$  matrix. This is one of the causes that could explain why different method produces similar coil patterns. For this reason we believe that through studying new geometries, novel gradient coil solutions can be found.

One of the concerns of symmetry-free gradient coil design methods is the high computational burden. The discrete nature of the approach requires the repeated evaluation of expressions that contain surface integrals [23]–[26]. In the present approach, the expressions (15)–(18), may be approximated to line integrals. Another advantage of the EMC relates to the possibility of extending the method as a shape optimization approach [30], [31]. Using the relationship between stream function and magnetization-thickness function (9), we realize that given the stream function value the thickness  $h$  may be changed for a given fixed magnetization. The possibility of changing the magnetization sign and value could limit the practical implementation of fixing the thickness, and change

the magnetization for the given objective function and linear field constraints. Another possibility is the design of the hybrid system where current and magnetized iron may coexist. The EMC produces a magnetization-thickness-current map and the designer may decide which region of the solution domain will be filled with current or magnetized iron.

The software GMSH [32] was used as a mesh generator in this research. GMSH is an automatic 3-D finite element grid generator with a built-in CAD engine and post-processor. It provides a simple meshing tool for academic problems with parametric input and advanced visualization capabilities. In order to solve the problem stated in (19) we employed the function *quadprog* provided in the MATLAB optimization toolbox. The function returns the optimal stream function amplitudes that minimize the equivalent magnetic energy and at the same time produces the desired target field. More sophisticated algorithms based on stochastic optimization technique [21] might be used in order to avoid local minimal solutions at the expense of computational time.

In order to validate the impedance calculation, the software FastHenry [33] was used. FastHenry is a multipole-accelerated impedance extraction program that takes the wires and their thickness to model the inductance and resistance of the coil.

Using the stream function concept the discrete wires are placed at equally spaced contours of the stream function values [3], [12]. The magnetic field and gradient magnitudes are evaluated by applying the Biot-Savart law to the wire segments coordinates extracted from the contour information.

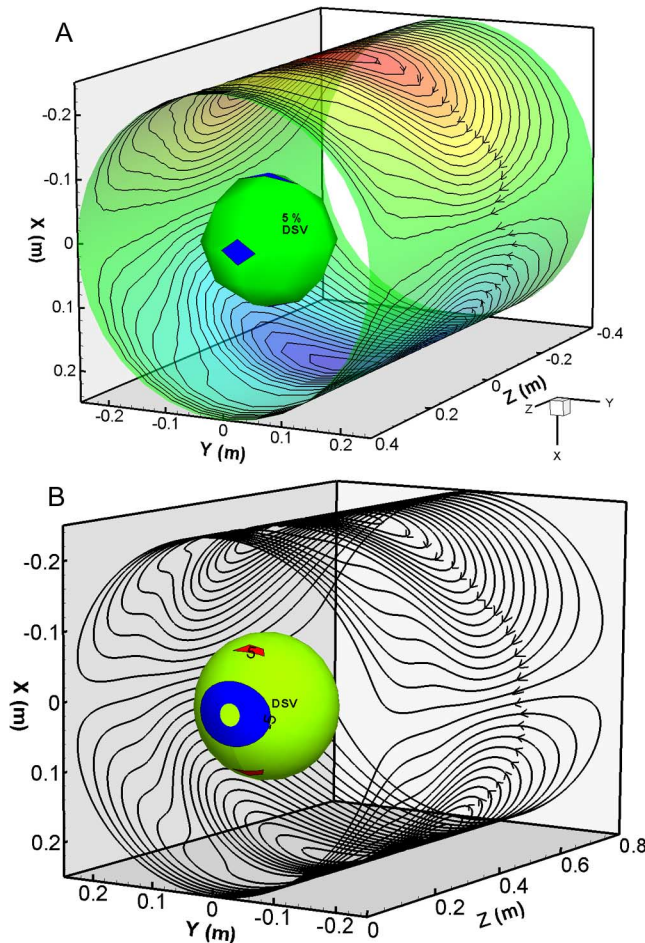


Fig. 3. Asymmetric transverse gradient coil designed with the EMC (a) and the solution generated by the relaxed target field method [19]. The 5% contour of the gradient nonuniformity is also shown. The arrow head indicates the sense of the current in the coil. The coil pattern (a), (b) shows similar topology.

### III. RESULTS AND DISCUSSIONS

We applied the EMC method for asymmetric transverse gradient coil, shielded three-dimensional transverse and longitudinal gradient coils for horizontal and biplanar magnets. The objective of this section was to demonstrate the versatility of the EMC method and the possibility of to be applied to a wide range of geometries and target spatial field characteristic.

For comparison, the Figure-of-Merit (FOM)  $\eta^2/L$  was used as a measurement of coil performance [1], [17]. The nonlinearity and nonuniformity of the gradient strength were calculated using (24–27) in [34]. The maximal field deviation ( $\Delta B_z^{\max}$ ) from the lineal target field was calculated using [26, Eq. (3)].

Fig. 2 shows the three geometries and triangular meshes generated for the examples. A uniform thickness was set to  $h = 3$  mm for all the examples and a 3 mm diameter wire was used for resistance calculation. We choose the power minimization as the objective function for the optimization problem (19).

#### A. Asymmetric Unshielded Transverse Gradient Coil

In this example we show the ability of the EMC method to generate coil that produces a linear magnetic field within an axially shifted target DSV.

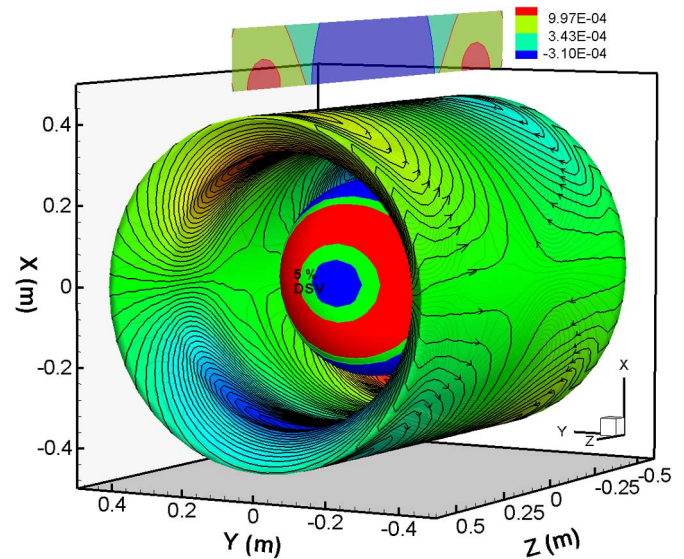


Fig. 4. Ultra-short shielded transverse gradient coil. The 5% deviation of the target gradient is shown on the surface of the DSV. The field plot contour in the top of the coil shows the values of the axial component of the magnetic field (in Tesla) at the shielding target surface. The arrow head indicates the sense of the current in the coil.

The geometry is a cylinder of radius 25 cm, 80 cm in length. The surface was discretized into 1280 triangles and 672 nodes. The DSV was shifted 25 cm from the cylinder center along the axial direction and 360 target points were set on DSV surface being 21 cm diameter. The target magnetic field gradient,  $G_0$ , was set to  $10 \cdot 10^{-3}$  T/m with an operating current of 100 A. The relaxing factor  $\varepsilon$  was set to 5% of deviation from the target  $G_0$  and no shielding condition or torque constraints were specified in this example.

In order to validate the result generated by the EMC method, an asymmetric fingerprint design was calculated using the relaxed target field method [19]. The same constraints and geometry were used for both methods for fair comparison.

Fig. 3(a) shows the coil current pattern generated with the EMC method. Approximately 82 s was taken by a Dual Core Pentium Laptop @ 2.00 GHz for the  $L_{mn}$  and  $R_{mn}$  matrix calculation; the same time was required for the evaluation of (13) and (17), (18). The computing time may change depending on the number of nodes used and the number of target points specified in the region of interest. Usually, the matrix energy evaluation consumes up to 50% of the total time. The coil was calculated and evaluated in no more than 3 min.

The FOM was  $0.38 \cdot 10^{-4}$  ( $T^2 \cdot m^{-2} \cdot A^{-2} \cdot H^{-1}$ ) and the gradient nonlinearity and nonuniformity in DSV was 1.09% and 2.63%, respectively. The calculated inductance using a filamentary wire approach [28] was 260.8  $\mu H$  and the value reported by the software FastHenry [33] was 264.6  $\mu H$ . The distance from the coil entrance to the 5% nonuniformity contour was 5.8 cm. Fig. 3(a) shows the shifted DSV and the spatial quality of the generated magnetic field. The same number of turns were used to generate  $10 \cdot 10^{-3}$  T/m in the design presented in Fig. 3(b). The FOM of this configuration was  $0.37 \cdot 10^{-4}$  ( $T^2 \cdot m^{-2} \cdot A^{-2} \cdot H^{-1}$ ), slighter smaller than the same value generated by the EMC coil. Both coils (A and B) generate a torque of 8.7

TABLE I  
CHARACTERISTIC OF THE ULTRA-SHORT GRADIENT COIL

Properties	Values
Stream function Contour	50
Current for $30 \cdot 10^{-3}$ T/m(A)	416.56
Efficiency $\eta$ ( $\mu$ T $m^{-1}$ $A^{-1}$ )	72.02
Nonlinearity, nonuniformity (%)	3.98, 3.46 ( <b>rms</b> )
Max. Field error, $\Delta \mathbf{B}_z^{\max}$ (%)	5
Inductance, L ( $\mu$ H)	695.05 (715.02)
Resistance (3 mm round wire), R (m $\Omega$ )	583.61 (582.12)
FOM, $\eta^2/L$ ( $T^2 \cdot m^{-2} \cdot A^{-2} \cdot H^{-1}$ )	$7.46 \cdot 10^{-6}$
$x$ -Torque, $T_x$ ( $N \cdot m \cdot A^{-1} \cdot T^{-1}$ )	$8.3 \cdot 10^{-5}$
$y$ -Torque, $T_y$ ( $N \cdot m \cdot A^{-1} \cdot T^{-1}$ )	$7.6 \cdot 10^{-5}$
$ \mathbf{B} _{\max}$ , @ DSV surface (mT)	7.15

Bracketed values of inductance and resistance were calculated using FastHenry [33].

$N \cdot m/A$  along the  $y$ -direction when the coils are immersed in a homogenous magnetic field ( $\mathbf{B}_0$ ) of 1.5 T. If the torque is included as a linear constraint in (19), then the resulting balanced solution produces a torque of  $-0.009 N \cdot m/A$  along the  $y$ -direction with a consequent reduction of 4.6 times in FOM. We used the Gauss-Legendre quadrature [35] for the evaluation of (13). Usually more elements are required in curved surface. Moreover, the more rapid the target field variation, the more triangular elements are required.

### B. Ultra-Short Shielded Transverse Gradient Coil

The second example consisted of designing a whole-body, ultra-short, shielded, transverse gradient coil. A similar structure was used for comparison purposes in a recently presented method [26]. The structure comprises a short primary cylinder and a longer secondary shielding cylinder joined by two conical sections. See Fig. 2(b). The geometry and method details can be found in [11], [26]. It was demonstrated that the conical surface provides the possibility of joining the primary current pattern with the shielding coil, hence the short-coil and high performance design can be obtained [26]. In this example we demonstrate that the EMC method generates high performance three-dimensional coil structures. Fig. 4, depicts the coil pattern obtained with the EMC method.

In a similar way to the solution obtained in [26], the current path on the conical surface flows in a convenient way to minimize the power and at the same time producing the desired magnetic field in the region of interest. If the same coil dimensions are used for a conventional shielded cylindrical geometry (no connected primary and secondary coils) then a high concentration of wires appear at the ends of the coil to provide return paths for the wire loops. This fact increases the cooling problems of such a coil and for a fixed minimum wire spacing reduces the coils efficiency. Table I shows the electromagnetic characteristics of the EMC ultra-short shielded gradient coil.

In the design we have specified 144 target points on the shielding surface and we have included this field condition as linear constraints as seen in (19). Fig. 4 shows, above the coil,

the contour values in Tesla corresponding to the axial magnetic field component outside the active magnetic shield.

One of the characteristic of the EMC method appears to be that the current paths are less smooth than those generated by the conventional inverse boundary element method [26] (BEM) and considerably less than the methods based on analytical expression of the stream function [12]. The EMC method assumes a constant magnetization in each triangle (a zeroth-order approximation to the stream-function) and hence the conductor placement should theoretically follow the triangles edges. (This is because the curl of the stream-function is only non-zero at the edges of the triangles). Linear interpolation of the stream-function between nodes is performed here to obtain a smooth current pattern. By assuming a linear variation of the magnetization in each triangle this intermediate step can be avoided, this will form the focus of our future research.

### C. Partially Shielded, Three-Dimensional, Biplanar Coil Design

The design of shielded biplanar gradient coils is more challenging than designing shielded cylindrical coils for whole body magnets. The biplanar structure surrounds the DSV to a lesser extent than the closed cylindrical structures. Hence, to generate the same magnetic field, more current is needed in biplanar coils for the same DSV. Moreover, new MRI techniques require increased magnetic field gradient strengths and larger numbers of turns have to be fitted in a spatially-restricted primary coil whose radius is approximately 42 cm.

In order to maximize the main field strength  $\mathbf{B}_0$  the distance between the two pole faces are reduced and the available space for the gradient coil set is highly restricted. This space constraint greatly limits the ability to produce well-shielded, highly linear gradient coils with high efficiency and low inductance.

Circular and rectangular planar geometries have previously been employed for biplanar coils [36]–[46]. However, we consider that more effort can be dedicated to the design of planar geometry gradient coils. Using the EMC method, in combination with a three-dimensional planar structure, we demonstrate that it is possible to obtain superior solutions for shielded transverse and longitudinal biplanar gradient coils. The geometry (C) in Fig. 2 was used for this purpose. We used the same coil dimension reported in [47].

The structure consists of four parallel planes. The two primary coils are located at  $z = \pm a$  and the shielding coils at the two outer planes, placed at  $z = \pm b$ . The inner and the outer circular planes are joined through a conical surface. The DSV was set to 35 cm, the radius of the primary and secondary coils was set to 42 cm and 50 cm respectively and the planes were located at  $Z = \pm 23$  cm and  $Z = \pm 29$  cm respectively.

A weak shielding condition was specified at  $Z = \pm 30$  cm for the transverse and the longitudinal biplanar gradient coils. If a strong shielding constraint is specified then solutions with high oscillating current pattern are generated and hence a lower efficiency and complex coils winding are produced. If no shielding constraint is specified then a conventional two-layer unshielded biplanar coil is obtained. A partially shielded biplanar gradient coil offers the best tradeoff between shielding-FOM and building complexity. See Fig. 5. This kind

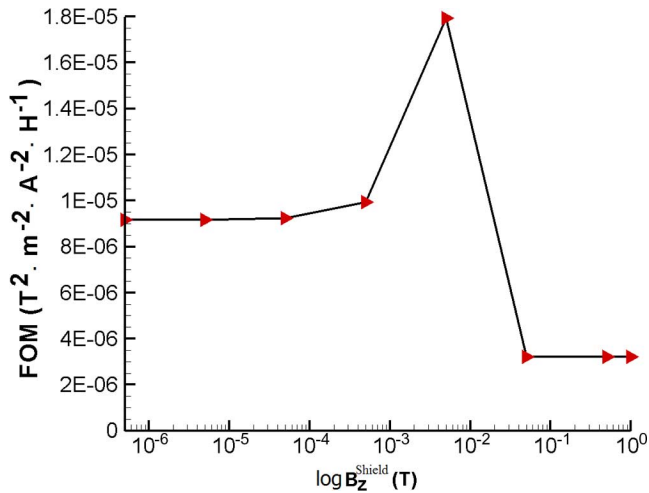


Fig. 5. Magnetic field shielding constraints versus FOM. The curve shows the change in FOM from strong up to weak shielding constraints. The maximal value of FOM is produced by a coil where few return current paths are generated outside of the coil center. This produces an improvement in coil efficiency and FOM.

of solutions produces few reversal turns at the secondary coils and hence high performance coil is obtained. Fig. 6(a), (b) depicts the three-dimensional coil profiles and Table II presents the coil parameters.

Fig. 6(a) shows that the remaining closed turns in the primary and in the secondary planes contribute to the magnetic field at the DSV.

The turn that flows from the primary to the shielding coil contribute to the DSV and at the same time act as a shielding in the outer coil. Some of the turns of the primary coil flow on the cone surface and hence the dissipated power is better distributed and more inter-space wire is available and less build complexity is presented. Comparing the biplanar transverse gradient coil efficiency with the biplanar shielded coil presented in [47], we realize that the solution presented in this paper is 1.24 times more efficient than the configuration presented in [47]. This type of profile generates a partially shielding effect and at the same time produces high performance biplanar transverse gradient coils. Fig. 6(b) presents the partially shielded biplanar longitudinal gradient coil.

#### IV. CONCLUSIONS

A new method for designing, independent of the shape of the current-carrying surface, gradient coils has been presented.

The known stream function and EMC concepts have been applied to the design of gradient coils of arbitrary shape. Assuming a constant magnetization-thickness function in each element and applying the equivalence between current and magnetization the equivalent stored magnetic energy, force, torque and coil resistance can be calculated. The EMC approach simplifies the model calculation using line integrals and hence less computational burden is required. Similar coil characteristics are generated when a referenced solution is designed using the EMC method. With the examples shown in this paper we have demonstrated high performance gradient coils with complex geometry and highly asymmetric target fields can be generated

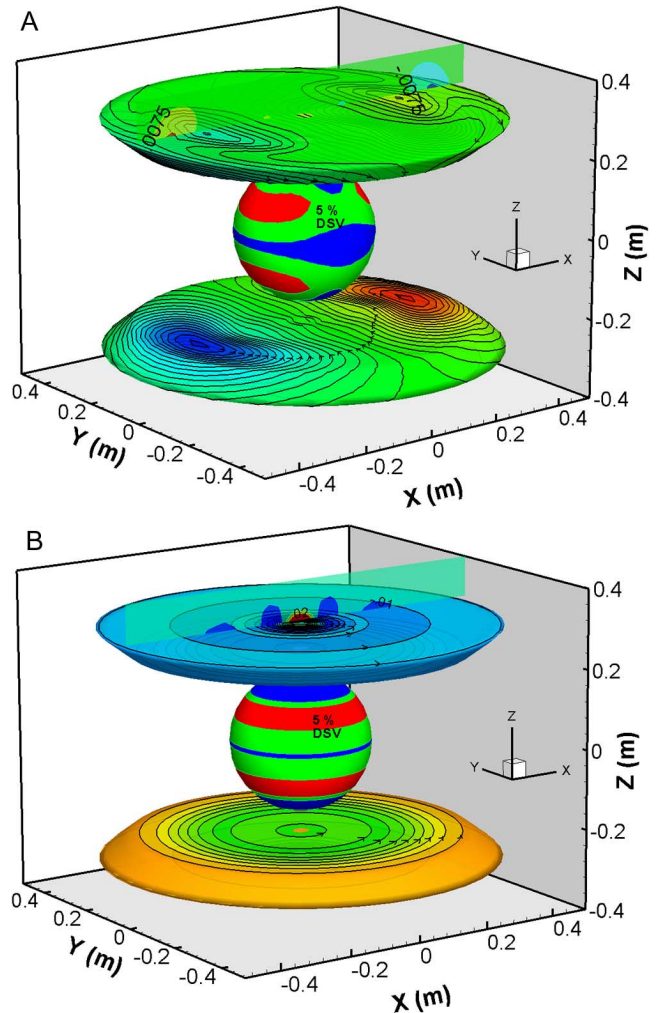


Fig. 6. Three-dimensional biplanar transverse (a) and longitudinal (b) gradient coil designs. The 5% contour of the gradient nonuniformity is also shown. The wire flows off from the primary surface toward the shielding surface. Contours of the axial component of the magnetic field (in Tesla) are shown at the top of the upper shielding coil.

TABLE II  
CHARACTERISTIC OF THE BIPLANAR GRADIENT COIL DESIGNS

Properties	Values	
	Transverse	Longitudinal
Stream function Contour (one half)	36	20
Current for $30 \cdot 10^{-3}$ T/m(A)	395.4	488
Efficiency $\eta$ ( $\mu$ T $\cdot$ m $^{-1}$ $\cdot$ A $^{-1}$ )	75.87	61.46
Nonlinearity, nonuniformity (%)	1.11, 2.67(rms)	2.12, 3.18(rms)
Max. Field error, $\Delta B_z^{\max}$ (%)	3.46	4.86
Inductance, L ( $\mu$ H)	317.49 (326.29)	95.4 (100.4)
Resistance, R (m $\Omega$ )	236.35 (228.6)	133.72 (130.14)
FOM, $\eta^2/L$ (T $^2$ $\cdot$ m $^{-2}$ $\cdot$ A $^{-2}$ $\cdot$ H $^{-1}$ )	$18.13 \cdot 10^{-6}$	$39.60 \cdot 10^{-6}$
$ \mathbf{B} _{\max}$ , @ DSV surface (mT)	5.6	4.5

Bracketed values of inductance and resistance were calculated using FastHenry [33]

using this approach. Applying the EMC method a new partially shielded biplanar transverse and longitudinal gradient coil has

been presented. Due to the equivalence between the magnetization-thickness and stream function the EMC may be extended to shape optimization techniques and hybrid designs (iron and current).

#### ACKNOWLEDGMENT

This work was supported by the Australian Research Council.

#### REFERENCES

- [1] J. W. Carlson, K. A. Derby, K. C. Haveryszko, and M. Weideman, "Design and evaluation of shielded gradient coils," *Magn. Reson. Med.*, vol. 26, pp. 191–206, 1992.
- [2] P. Mansfield and B. Chapman, "Active magnetic screening of coils for static and time-dependent magnetic field generated in NMR imaging," *J. Phys. E*, vol. 19, pp. 540–545, 1986.
- [3] R. Turner, "Gradient coil design: A review of methods," *Mag. Reson. Imag.*, vol. 11, pp. 903–920, 1993.
- [4] R. Bowtell and P. Mansfield, "Gradient coil design using active magnetic screening," *Magn. Reson. Med.*, vol. 17, pp. 15–21, 1991.
- [5] P. B. Roemer and J. S. Hickley, *Self-Shielded Gradient Coils for Nuclear Magnetic Resonance Imaging* U.S., 1986.
- [6] M. A. Morich, *MRI Self-Shielded Gradient Coils U.S.*, 1992.
- [7] C. Eccles, S. Crozier, W. Roffmann, D. Doddrell, P. Back, and P. Callaghan, "Practical aspects of shielded gradient-coil design for localized in vivo NMR spectroscopy and small-scale imaging," *Magn. Reson. Imag.*, vol. 4, pp. 621–630, 1994.
- [8] S. Crozier and D. Doddrell, "A design methodology for short, whole-body, shielded gradient coils for MRI," *Magn. Reson. Imag.*, vol. 4, pp. 615–620, 1995.
- [9] B. Chronik and B. R. BK, "Constrained length minimum inductance gradient coil design," *Magn. Reson. Med.*, vol. 39, pp. 270–278, 1998.
- [10] S. Shvartsman, R. Brown, Y.-C. Cheng, T. Eagan, and H. Fujita *et al.*, "A new "supershielding" method applied to the design of gradient coils," *Magn. Reson. Med.*, vol. 45, pp. 147–155, 2001.
- [11] S. H. Shvartsman, M. Morich, G. Demeester, and Z. Zhai, "Ultrashort shielded gradient coil design with 3D geometry," *Concepts Magn. Reson.*, vol. 26B, pp. 1–5, 2005.
- [12] M. A. Brideson, L. K. Forbes, and S. Crozier, "Determining complicated winding patterns for shim coils using stream functions and the target-field method," *Concepts Magn. Reson.*, vol. 14, pp. 9–18, 2002.
- [13] P. Mansfield, "Multi-planar image formation using NMR spin echoes," *J. Phys. C*, vol. 10, pp. L55–L58, 1977.
- [14] A. M. Abduljalil, A. H. Aletras, and P.-M. L. Robitaille, "Torque free asymmetric gradient coils for echo planar imaging," *Magn. Reson. Med.*, vol. 31, pp. 450–453, 1994.
- [15] D. C. Alsop and T. J. Connick, "Optimization of torque-balanced asymmetric head gradient coils," *Magn. Reson. Med.*, vol. 35, pp. 875–886, 1996.
- [16] S. Crozier, K. Luescher, G. Hinds, W. U. Roffmann, and D. M. Doddrell, "Designs for an asymmetric gradient set and a compact superconducting magnet for neural magnetic resonance imaging," *Rev. Sci. Instrum.*, vol. 70, pp. 4062–4066, 1999.
- [17] B. A. Chronik, A. Alejski, and B. K. Rutt, "Design and fabrication of a three-axis edge ROU head and neck gradient coil," *Magn. Reson. Med.*, vol. 44, pp. 955–963, 2000.
- [18] D. Tomasi, R. F. Xavier, B. Foerster, H. Panepucci, A. Tannús, and E. L. Vidoto, "Asymmetrical gradient coil for head imaging," *Magn. Reson. Med.*, vol. 48, pp. 707–714, 2002.
- [19] H. Sanchez, F. Liu, A. Trakic, and S. Crozier, "A simple relationship for high efficiency-gradient uniformity tradeoff in multi-layer asymmetric gradient coils for MRI," *IEEE Trans. Magn.*, vol. 43, pp. 523–532, 2007.
- [20] J. Leggett, D. Green, and R. Bowtell, "Insert dome gradient coils for brain imaging," presented at the 14th Annual Meeting of ISMRM, Seattle, WA, 2006, unpublished.
- [21] S. Crozier and D. DM, "Gradient coil design by simulated annealing," *J. Magn. Res.*, vol. A 103, pp. 354–357, 1993.
- [22] H. Sanchez, F. Liu, A. Trakic, E. Weber, and S. Crozier, "Three-dimensional gradient coil structures for magnetic resonance imaging designed using fuzzy membership functions," *IEEE Trans. Magn.*, vol. 43, pp. 3558–3566, 2007.
- [23] S. Pissanetzky, "Minimum energy MRI gradient coils of the general geometry," *Meas. Sci. Technol.*, vol. 3, pp. 667–673, 1992.
- [24] G. N. Peeren, "Stream function approach for determining optimal surface currents," *J. Comput. Phys.*, vol. 191, pp. 305–321, 2003.
- [25] R. A. Lemdiasov and R. Ludwig, "A stream function method for gradient coil design," *Concepts Magn. Reson. B*, vol. 54, pp. 656–668, 2005.
- [26] M. Poole and R. Bowtell, "Novel gradient coils designed using a boundary element method," *Concepts Magn. Reson. B*, vol. 31B, pp. 162–175, 2007.
- [27] T. Preston and A. Reece, "Solution of 3-D eddy current problems the T-method," *IEEE Trans. Magn.*, vol. 18, pp. 486–491, 1982.
- [28] J. D. Jackson, *Classical Electrodynamics*, 3rd ed. New York: Wiley, 1998.
- [29] S. Shvartsman and M. C. Steckner, "Discrete design method of transverse gradient coils for MRI," *Concepts Magn. Reson. B*, vol. 31, pp. 95–115, 2007.
- [30] N. D. Derek and A. L. David, "Automated design of magnetic devices by optimizing material distribution," *IEEE Trans. Magn.*, vol. 32, pp. 1188–1193, 1996.
- [31] H. Sanchez Lopez, F. Liu, E. Weber, and S. Crozier, "Passive shim design and a shimming approach for biplanar permanent magnetic resonance imaging magnets," *IEEE Trans. Magn.*, vol. 44, pp. 394–402, 2008.
- [32] C. Geuzaine and J.-F. Remacle, *Gmsh Reference Manual: The Documentation for Gmsh, a Finite Element Mesh Generator With Built-In Pre-and Post-Processing Facilities* [Online]. Available: <http://www.geuz.org/gmsh/> 2008
- [33] M. Kamon, M. Tsuk, and J. White, "FastHenry: A multipole-accelerated 3-D inductance extraction program," *IEEE Trans. Microwave Theory Tech.*, vol. 42, pp. 1750–1758, 1994.
- [34] S. M. Shvartsman, R. W. Brown, Y. C. Cheng, T. P. Eagan, H. Fujita, M. A. Morich, L. S. Petropoulos, and J. D. Willig, "Application of the SUSHI method to the design of gradient coils," *Magn. Reson. Med.*, vol. 45, pp. 147–55, 2001.
- [35] H. T. Rathod, K. V. Nagaraja, B. Venkatesudu, and N. L. Ramesh, "Gauss Legendre quadrature over a triangle," *J. Indian Inst. Sci.*, vol. 84, pp. 183–188, 2004.
- [36] K. Yoda, "Analytical design method of self-shielded planar coils," *J. Comput. Phys.*, vol. 67, pp. 4349–4353, 1990.
- [37] M. A. Martens, L. S. Petropoulos, R. W. Brown, J. H. Andrews, M. A. Morich, and J. L. Patrick, "Insertable biplanar gradient coils for magnetic resonance imaging," *Rev. Sci. Instrum.*, vol. 62, pp. 2639–2645, 1991.
- [38] B. J. Fisher, N. Dillon, T. A. Carpenter, and L. D. Hall, "Design of a biplanar gradient coil using a genetic algorithm," *Magn. Reson. Imag.*, vol. 15, no. 3, pp. 369–376, 1997.
- [39] H. Liu, "Finite size bi-planar gradient coil for MRI," *IEEE Trans. Magn.*, vol. 34, pp. 2162–2164, 1998.
- [40] E. C. de Caparelli, D. Tomasi, and H. Panepucci, "Shielded biplanar gradient coil design," *J. Magn. Reson. Imag.*, vol. 9, pp. 725–731, 1999.
- [41] C. H. Moon, H. W. Park, M. H. Cho, and S. Y. Lee, "Design of convex-surface gradient coils for a vertical-field open MRI system," *Meas. Sci. Technol.*, vol. 11, pp. N89–N94, 2000.
- [42] L. S. Petropoulos, "Finite size disc gradient coil set for open vertical field magnets," *Magn. Reson. Imag.*, vol. 18, pp. 615–624, 2000.
- [43] L. Forbes and S. Crozier, "Novel target-field method for designing shielded biplanar shim and gradient coils," *IEEE Trans. Magn.*, vol. 40, pp. 1929–1938, 2004.
- [44] L. Forbes, M. Brideson, and S. Crozier, "A target-field method to design circular biplanar coils for asymmetric shim and gradient fields," *IEEE Trans. Magn.*, vol. 41, pp. 2134–2144, 2005.
- [45] V. Vegh, H. W. Zhao, G. J. Galloway, D. M. Doddrell, and I. M. Brereton, "The design of planar gradient coils. Part I: A winding path correction method," *Concepts Magn. Reson.*, vol. 27B, no. 1, pp. 17–24, 2005.
- [46] F. Qi, X. Tang, W. M. Wang, Y. F. Shen, S. P. Liu, and Z. D. Jiang, "A new simulated annealing method of designing NMR biplanar shim coils," *Progr. Nat. Sci.*, vol. 16, no. 7, pp. 747–752, 2006.
- [47] W. Liu, D. Zu, X. Tang, and H. Guo, "Target-field method for MRI biplanar gradient coil design," *J. Phys. D: Appl. Phys.*, vol. 40, pp. 4418–4424, 2007.